

Experimental and Quantum Chemical Calculations of Imidazolium Appended Naphthalene Hybrid in Different Biomimicking Aqueous Interfaces

Tej Varma Yenupuri,^{*,†} Lucia Mydlova,[‡] Devesh S. Agarwal,[§] Ritika Sharma,[†] Rajeev Sakhuja,[§] Malgorzata Makowska-Janusik,^{*,‡} and Debi D. Pant^{*,†}

[†]Department of Physics, Birla Institute of Technology and Science (BITS) Pilani, Pilani 333031, Rajasthan, India

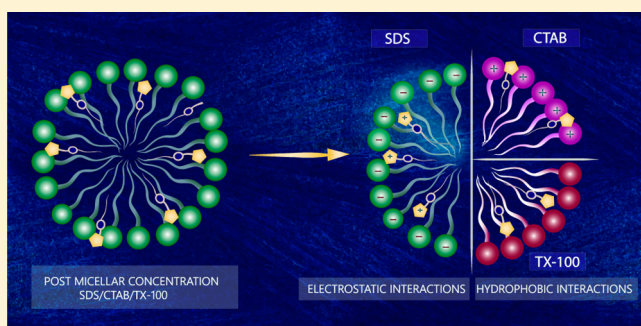
[‡]Institute of Physics, Faculty of Mathematics and Natural Science, Jan Dlugosz University, Al. Armii Krajowej 13/15, 42-200 Czestochowa, Poland

[§]Department of Chemistry, Birla Institute of Technology and Science (BITS) Pilani, Pilani 333031, Rajasthan, India

S Supporting Information

ABSTRACT: The effect of solvent polarity and micellar headgroup on a newly designed imidazolium based ionic liquid (IL) conjugated with naphthalene, 1,2-dimethyl-3-((6-(octyloxy)naphthalen-2-yl)methyl)-1*H*-imidazol-3-ium chloride (IN-O8-Cl), was studied using steady state and time-resolved fluorescence techniques. We observed that the dipole moment in the excited state is remarkably higher than the ground state. The effect of micellar surface charge on the photophysics of IN-O8-Cl in aqueous phase at room temperature was investigated. Formation of pre-micellar aggregates in sodium dodecylsulfate (SDS) was perceived; further the microenvironment of IN-O8-Cl was examined

using steady-state fluorescence spectroscopy. Micropolarity of the micellar environment of SDS was found to be lower than that of cetyltrimethylammonium bromide (CTAB) and triton X-100 (TX100) following the order SDS < TX-100 < CTAB. The binding constant (K_b) and edge excitation red shift (EERS) from the emission maximum suggest that the probe binds strongly to the micelles. Multiexponential behavior was observed in time-resolved fluorescence lifetime studies in all micellar environments. We have observed an increase in rotational correlation time as we move from pure aqueous phase to solution containing surfactants of different head charge. Varieties of spectral parameters were used to justify the region in which the probe is present. The experimentally obtained dipole moment data were justified and explained by the DFT calculations of the electronic properties of IN-O8-Cl molecules in gas phase and in selected solvents.



1. INTRODUCTION

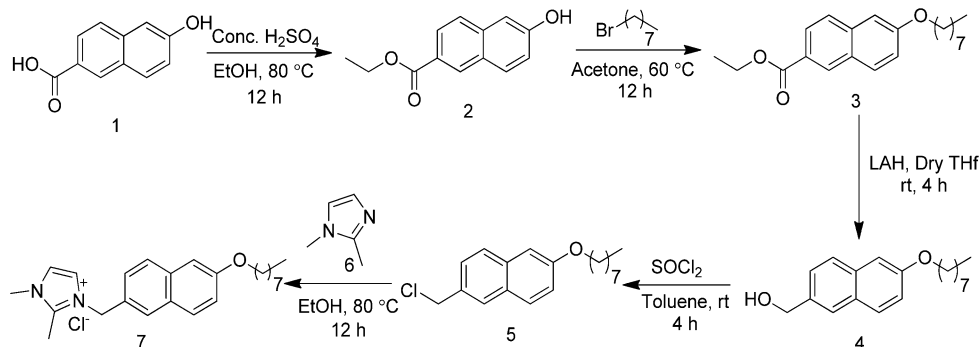
Fluorescence techniques have been successfully employed for the investigation of different fundamental processes in biological systems due to their capability for rapid, precise, conscientious, and reproducible detection of proteins and biomolecules at the single-molecule level.^{1,2} Concrete efforts have been devoted to fluorescence labeling, sensing, and quantification of proteins and other biomolecules by fluorescent organic dyes and their derivatives.^{3,4} It has been attributed to the diversified spectral properties possessed by mentioned fluorescent probes and the ease of their structural modification. Although, a variation in fluorescence intensity or a deviation in the fluorescence band is usually accompanied by interaction of a fluorescent probe with a protein or biomolecule, irreversible photobleaching during prolonged illumination and lack of photostability reduces effective sensing of these organic molecules.³ A large number of fluorescein and rhodamine dyes, most cyanine dyes, and 4,4'-difluoro-4-bora-3a,4a-diaza-s-indacene dyes possess comparatively exiguous

absorption and fluorescence bands and also minor Stokes shift to change in solvent polarity, high molar-absorption coefficient, and modest quantum yield.⁴ In addition, with very few exceptions, such as acridone dye,⁵ the fluorescence decay lifetime is in the range of about 5 ns in the visible region and around 1 ns in the infrared region for numerous organic dyes and usually is short-lived for efficient temporal discrimination from cellular autofluorescence and scattered excitation light by isolation or temporarily blocking a portion of time, thereby lowering the sensitivity.⁵ Also, the function of biomolecules might get influenced due to structure, charge, and hydrophilicity of organic dye. In addition, complex and tedious preparation and workup methodologies, low yields, and poor water-solubility limit the practical applicability of these fluorescent probes for sensing proteins and biomolecules in

Received: June 10, 2016

Revised: July 27, 2016

Scheme 1. Synthesis of 1, 2-Dimethyl-3-((6-(octyloxy)naphthalen-2-yl)methyl)-1H-imidazol-3-ium Chloride (IN-O8-Cl).



real biological environments.^{6,7} Hence development of alternate fluorescence probes for sensing in water or biological environment is highly desirable.

Efforts toward improving the water solubility of these organic molecules have led to design of ionic liquid-based fluorescent probes.^{8–10} More specifically, the use of room-temperature ionic liquids (RTILs) is more favorable due to their large size, excellent thermal stabilities, conformational flexibility of the ions, and controllable physical and chemical properties¹¹ that favor the liquid state.¹² In addition acting as environmentally benign solvent systems, ionic liquids have been utilized recently as designer substrates for preparing functionalized materials.^{13–15} The physical chemistry of imidazolium-based ionic liquids have been investigated due to their particular dimensional heterogeneity emerging from the internal polar/nonpolar segregation. These molecules exhibit fluorescence when they are excited in the ultraviolet or initial visible region, and the excitation wavelength plays a crucial role in the fluorescence behavior due to the existence of analytically different correlated forms of the fundamental ions of the ionic liquids that prolong the relaxation of the excited state in these solutions.^{16,17} Chen and co-workers reported the use of ILs as potential fluorescent probes^{18,19} for the sensing of biomacromolecules.¹⁹ Subsequently, Liu et al.²⁰ studied a novel functional fluorescent imidazolium-based IL probe for detecting superoxide anion radicals. Recently, Galpothdeniya and co-workers reported a fluorescein-based IL sensor for label-free detection of serum albumins.²¹ IL-based materials have also been utilized for detection of vapors and for estimation of the pH value.^{22,23}

Despite the significant potential of imidazolium-based ILs for sensing of biomolecules, their use as fluorescence probes is still limited due to their low fluorescence efficiency. To the best of our knowledge, the fluorescent efficacy of imidazolium-based fluorescent probes has not been much explored in different micellar environments. In the context of the above discussions, we herein report the synthesis of a highly fluorescent naphthalene-appended imidazolium-based IL, whose fluorescent intensity could be significantly increased or quenched upon addition of surfactants. The high fluorescence efficiency imparted by the naphthalene moiety²⁴ and the hydrophilic nature of the IL makes it a favorable fluorescent probe candidate for effective sensing of proteins and biomolecules in different well-known biomimicking environments of micelles.

2. EXPERIMENTAL SECTION

2.1. Materials. Synthesis of 1,2-dimethyl-3-((6-(octyloxy)-naphthalen-2-yl)methyl)-1H-imidazol-3-ium chloride (IN-O8-Cl) is presented in Scheme 1.

2.1.1. Synthesis of Ethyl 6-Hydroxy-2-naphthoate (2). To a stirred solution of 1 (10.6 mmol) in ethanol, conc H₂SO₄ (0.02 mmol) was added at 0 °C, and the reaction mixture was heated at 80 °C for 12 h. After consumption of starting material as determined by TLC, the solvent was evaporated under reduced pressure, and 2 N NaHCO₃ (30 mL) solution was added at 0 °C. The precipitate was filtered under suction to yield product (2) as an off white solid, which was used as such without any further purification. Yield: 92% (2.11 g); mp 110–110.6 °C.

2.1.2. Synthesis of Ethyl 6-(Octyloxy)-2-naphthoate (3). To a stirred solution of 2 (9.2 mmol) in acetone, K₂CO₃ (20.2 mmol) was added at 0 °C. The reaction mixture was stirred for 15 min at 0 °C, after which 1-bromo octane (1.0 mmol) was added and the reaction was refluxed for 12 h. After completion of the reaction as determined by TLC, the solvent was removed under high pressure. The reaction was quenched by adding water (50 mL). The water layer was extracted using ethyl acetate (20 mL × 2). The ethyl acetate layer was dried over anhydrous sodium sulfate, and ethyl acetate was removed at high temperature and low pressure to give product 3 as colorless oil. Yield: 90.8% (2.75 g).

2.1.3. Synthesis of (6-(Octyloxy)naphthalen-2-yl)methanol (4). To dry THF (20 mL), LAH (22.8 mmol) was added and stirred at 0 °C for 15 min; to this, a solution of 3 (7.6 mmol) was added. After 4 h of stirring, complete consumption of starting material was observed by TLC. The reaction was quenched by adding 1 N NaOH solution (30 mL) after cooling the reaction mixture to 0 °C. Ethyl acetate (20 mL × 2) was added to the reaction solution, and the mixture was filtered through Celite. Subsequently mother liquor was separated into organic layer and water layer, and finally the organic layer was dried over anhydrous sodium sulfate, and ethyl acetate was evaporated at low temperature and high pressure to give product 4 as off white solid. Yield: 82.6% (1.80 g); mp 98.2–99.0 °C. ¹H NMR (400 MHz, CDCl₃) δ 7.76 (dd, *J* = 8.9, 4.7 Hz, 3H), 7.50 (dd, *J* = 8.5, 1.8 Hz, 1H), 7.25–7.20 (m, 2H), 4.77 (s, 2H), 4.11 (t, *J* = 6.6 Hz, 2H), 1.94–1.85 (m, 2H), 1.60–1.50 (m, 2H), 1.44–1.33 (m, 8H), 0.96 (t, *J* = 6.9 Hz, 3H). ¹³C NMR (101 MHz, CDCl₃) δ 151.27, 135.86, 134.17, 129.28, 128.68, 127.18, 125.81, 125.59, 119.34, 106.48, 68.06, 65.62, 31.85, 29.41, 29.28, 29.27, 26.14, 22.69, 14.14.

2.1.4. Synthesis of 2-(Chloromethyl)-6-(octyloxy)-naphthalene (5). At 0 °C to a solution of 4 (5.9 mmol) in toluene, SOCl₂ (89.0 mmol) was added. After 4 h, TLC showed the complete disappearance of the starting material. Toluene was removed under reduced pressure, and the reaction was quenched by adding NaHCO₃ solution (40 mL) to maintain the pH at 10, while cooling the reaction to 0 °C. The

sodium bicarbonate layer was extracted using ethyl acetate (20 mL \times 2). Finally the ethyl acetate layer was dried over anhydrous sodium sulfate, and the organic layer was concentrated at high pressure low temperature to give product **5** as colorless oil. Yield: 95.8% (1.73 g). ^1H NMR (400 MHz, CDCl_3) δ 7.74 (d, J = 8.3 Hz, 3H), 7.47 (dd, J = 8.6, 1.2 Hz, 1H), 7.20–7.13 (m, 2H), 4.84 (s, 2H), 4.09 (t, J = 6.6 Hz, 2H), 1.92–1.83 (m, 2H), 1.57–1.48 (m, 2H), 1.42–1.29 (m, 8H), 0.92 (t, J = 6.9 Hz, 3H). ^{13}C NMR (101 MHz, CDCl_3) δ 157.73, 134.46, 132.38, 129.41, 129.08, 128.27, 127.51, 126.81, 119.63, 106.51, 68.11, 46.93, 31.89, 29.45, 29.33, 29.28, 26.17, 22.74, 14.19.

2.1.5. Synthesis of 1, 2-Dimethyl-3-((6-(octyloxy)naphthalen-2-yl)methyl)-1H imidazol-3-ium Chloride (IN-O8-Cl) (7). To a stirred solution of 1,2 dimethyl imidazole (6.6 mmol) in ethanol (10 mL), **5** (5.5 mmol) was added, and the reaction mixture was heated at 80 °C for 12 h. The completion of the reaction was monitored by TLC. After the completion of the reaction, the solvent was evaporated under reduced pressure, and ethyl acetate (10 mL) was added to the crude product and stirred overnight. This process was repeated 3 times to remove excess of **6**, and finally the ethyl acetate was decanted, and the product was dried to give colorless oil, which became semisolid on standing. Yield: 92% (2.05 g). ^1H NMR (400 MHz, $\text{DMSO}-d_6$) δ 7.87–7.78 (m, 4H), 7.72 (d, J = 2.0 Hz, 1H), 7.42 (dd, J = 8.5, 1.6 Hz, 1H), 7.34 (d, J = 2.2 Hz, 1H), 7.19 (dd, J = 8.9, 2.4 Hz, 1H), 5.55 (s, 2H), 4.07 (t, J = 6.5 Hz, 2H), 3.78 (s, 3H), 2.65 (s, 3H), 1.80–1.73 (m, 2H), 1.47–1.41 (m, 2H), 1.35–1.20 (dd, J = 13.7, 6.8 Hz, 8H), 0.86 (t, J = 6.6 Hz, 3H). ^{13}C NMR (101 MHz, CDCl_3) δ 157.27, 145.12, 134.52, 130.06, 129.83, 128.52, 128.04, 127.20, 126.38, 123.21, 123.15, 121.75, 119.91, 107.02, 68.04, 51.21, 35.31, 31.72, 29.23, 29.16, 29.09, 26.04, 22.57, 14.14.

2.2. Computational Details. The initial geometry of the IN-O8-Cl molecule was built up using the ACD/ChemSketch software. Before calculation of its electronic properties, the geometry was optimized according to the energy minimization procedure applying the density functional theory (DFT) with DFT/B3LYP functional^{25,26} implemented in the Gaussian09 program package.²⁷ It was performed for molecule in vacuum using Berny algorithm²⁸ in redundant internal coordinates. The potential energy surface minimum was calculated by applying the restricted Hartree–Fock (RHF) methodology with the 6-31+G(d,p) basis set in C1 symmetry. The minimum of the energy in molecular ground state was checked by the absence of imaginary frequencies caring out the Hessian evaluation. It ensures the thermodynamic equilibrium of the molecule.

Subsequently, taking the same level of theory^{29,30} electronic and optical properties of IN-O8-Cl molecule were calculated. Namely, the HOMO and LUMO orbitals, as well as dipole moment, of the molecule in gas phase and in different solvents were evaluated. The solvent effect was taken into account using the polarizable conductor calculation model (CPCM)^{31,32} implemented under the self-consistent reaction field (SCRf) approach.^{33,34} For the studied molecule, also time dependent DFT (TD-DFT) calculations were carried out to investigate its excited state properties.

3. RESULTS AND DISCUSSION

3.1. Effect of Solvent on Absorption and Emission Spectra. Knowledge of the solvent effect on absorption and emission spectra is important, because the spectral behavior of molecules is related strongly to their electronic structure in the

excited and ground state. Thus, molecular changes in solvent are accompanied by changes in their polarity and in consequence by the evaluation of dielectric constant in the surrounding medium. Hence $F_1(\epsilon, \eta)$ and $F_2(\epsilon, \eta)$ are being used to determine the ground and excited state dipole moments from different organic solvents.

The molecular structure of the IN-O8-Cl molecule is shown in Figure S1. The absorption and fluorescence spectra of IN-O8-Cl (10^{-4} M) were measured at room temperature in various solvents. The absorption spectrum recorded for IN-O8-Cl dissolved in DMSO normalized to one is shown in Figure 1.

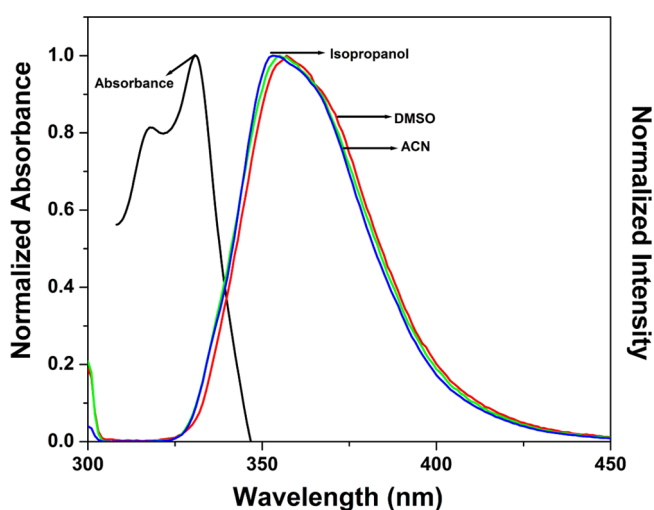


Figure 1. Normalized UV–vis absorption spectra measured in DMSO and normalized fluorescence spectra of IN-O8-Cl performed in DMSO, acetonitrile, and isopropanol.

The absorption band shows very low sensitivity (~ 1 nm) toward solvents with decreasing polarity. Hence one can conclude that solvent effects are negligible in the ground state of the molecule. The fluorescence emission spectra (see Figure 1 and Table S1) show one structured peak in all selected solvents. When the solvent polarity is increased from that of cyclohexane to that of water, the fluorescence peak is shifted toward longer wavelengths. This is caused by the strong intermolecular interactions occurring for the IN-O8-Cl being in the excited state in polar solvent environment. Moreover, the weak change in absorption spectra compared with that of the emission spectra indicates that the molecule is less polarized by the polar solvents in the ground state than in the excited state. These results firmly suggest that the nonbonding electrons are not involved in $n \rightarrow \pi^*$ transition but involved in $\pi \rightarrow \pi^*$ transition due to charge transfer.³⁵

3.2. Experimental Estimation of Ground and Excited State Dipole Moment. To get further insight on the solvatochromic behavior of the IN-O8-Cl, spectroscopic properties are correlated with relevant solvent polarities scales. Figure S2 shows $\bar{\nu}_a - \bar{\nu}_f$ versus $F_1(\epsilon, \eta)$, while Figure S3 shows $F_2(\epsilon, \eta)$ versus $\bar{\nu}_a + \bar{\nu}_f/2$. The linear behavior of the solvent polarity versus Stoke's shift demonstrates solvent effects as a function of refractive index and dielectric constant. The slopes of the fitted lines from Figure S2 and S3 were found to be $S_1 = 296$ and $S_2 = -363$, respectively. With the methodology and equations presented in our previous works,^{36–38} solute cavity radius (a_0) for IN-O8-Cl was found to be 5.75 Å, and calculated ground and excited state dipole moments of the

molecule are $\mu_g = 2.53$ D and $\mu_e = 24.95$ D, respectively. All data related to experimental dipole moment have been summarized in Table 1.

Table 1. Solute Cavity Radius, Slope of the Stoke's Shift Dependence vs Solvent Polarity, and Dipole Moment Data Measured for IN-O8-Cl in Ground and Excited States

molecule	a_0 (Å)	S_1 (cm^{-1})	S_2 (cm^{-1})	μ_g (D)	μ_e (D)	$\Delta\mu$ (D)	μ_e/μ_g
IN-O8-Cl	5.75	296	-363	2.53	24.95	22.42	9.86

The large increase in dipole moment of the excited state to that of the ground state is due to the redistribution of charge leading to conformational changes during excitation. This demonstrates that the molecule is much more polar in the excited state compared with the ground state. Also change in dipole moments on excitation indicates twisted intramolecular charge transfer (TICT) in the excited state. Due to ICT, the planarity of the molecular structure increases on excitation, leading to a high change in dipole moment. Seeing the change in ground and excited state dipole moments and the sensitivity of the emission spectra by varying the environment around the IN-O8-Cl, we decided to study this molecule in a more restricted environment using surfactants as an effect of head charge.

3.3. Computational Analysis. The properties of excited states of molecules play an important role in their chemical and physical behavior. As an example, many reactions can be initialized by electronic excitation or proceed via the excited state of the reactants. Excited states are important in many chemical processes, including photochemistry and electronic spectroscopy. Excitation of the molecule changes its charge distribution causing conformational changes. Both of these phenomena lead to alteration of dipole moment of the active molecule. Dipole moment of the excited state can increase or decrease compared with ground state.

The optimized structure of the IN-O8-Cl is presented in Figure 2. The molecule has a rod-like structure. One may see

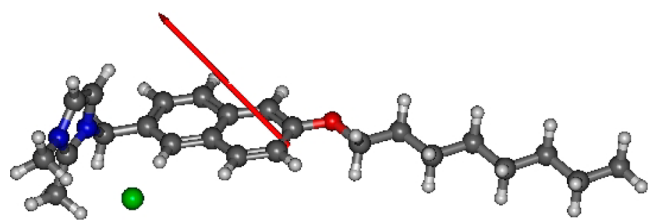


Figure 2. Gas phase optimized structure of the IN-O8-Cl molecule at B3LYP/6-31+G(d,p) level showing the overall dipole moment (red arrow).

that the naphthalene group is planar and simultaneously it is perpendicular to the imidazole group. The chlorine atom is located in the cage formed by naphthalene and imidazole planes. In Figure 2 is also presented location of the dipole moment of the IN-O8-Cl calculated at the B3LYP/6-31+G(d,p) level in gas phase. One may see that the dipole moment does not lie along the molecular structure but is positioned at an angle to its plane, which is caused by twisting of the imidazole group.

In Figure S4, the HOMO and LUMO orbitals of the ground state of the IN-O8-Cl molecule calculated at the B3LYP/6-31+G(d,p) level are presented. One may see that the HOMO orbital of the molecule in the gas phase is located at the chlorine atom and the electrons belonging to the naphthalene group create the LUMO orbital. All selected solvents change the nature of the HOMO orbitals leaving the LUMO orbitals unchanged. The selected solvents decrease the energy of HOMO and LUMO orbitals compared with the energies of these orbitals in the gas phase (see Table 2). The HOMO–LUMO energy difference forming the HOMO–LUMO energy gap splitting ($\Delta E_{\text{HOMO-LUMO}}$) for the molecule in different solvents is unchanged and is equal to 4.43 eV. In the gas phase, the $\Delta E_{\text{HOMO-LUMO}}$ is equal to 3.70 eV. This means that all of the selected solvents increase the $\Delta E_{\text{HOMO-LUMO}}$ of IN-O8-Cl. The selected solvents also increase the ground state dipole moment of the molecule. The level of growth of the dipole moment depends on the dielectric constant of the solvent. The higher the dielectric constant of the solvent, the greater is the change of the dipole moment of the molecule.

The shapes of the molecular electrostatic potential (MEP) of the IN-O8-Cl in ground state are reported in Figure S4. The electron density (per unit volume) is the greatest at the imidazole group in all solvents. In the case of gas phase, the electrons are more spread through the carbon chain. This means that the solvents move the electrons to the imidazole group causing the increase of its donating character. One may see that the more polar solvents more strongly move the electrons to the imidazole group. It is significantly seen in the case of water and DMSO solvents.

In Figure S5, the UV–vis absorption spectra calculated for the IN-O8-Cl molecule at B3LYP/6-31+G(d,p) level are presented. The first absorption peak obtained for the investigated molecule calculated in gas phase comes from HOMO to LUMO electron transfer. The second peak occurs from HOMO – 1 to LUMO electron absorption, while the HOMO – 1 orbital is located at the naphthalene group. Analyzing the UV–vis absorption spectra calculated in the solvent environment, one may see that they slightly depend on the solvent polarity. The investigated molecule demonstrates the hypsochromic shift for all selected solvents. This means that the IN-O8-Cl is negatively solvatochromic. The solvent

Table 2. Dipole Moment and HOMO and LUMO Energies Calculated for the IN-O8-Cl Molecule at the B3LYP/6-31+G(d,p) Level of Theory in Gas Phase and Selected Solvents

solvent	dielectric constant	ground state			first excited state		
		μ_g [D]	E_{HOMO} [eV]	E_{LUMO} [eV]	μ_e^1 [D]	E_{HOMO} [eV]	E_{LUMO} [eV]
gas phase		7.82	-4.58	-0.88	4.29	-2.93	-2.14
DCM	8.93	13.62	-5.60	-1.16	12.69	-5.40	-1.54
acetonitrile	35.69	15.09	-5.65	-1.22	14.84	-5.43	-1.59
DMSO	46.83	15.30	-5.66	-1.23	14.92	-5.43	-1.59
water	80.00	15.45	-5.66	-1.23	15.02	-5.44	-1.59

changes the intensity of the first absorption peak, because in the solvent environment the HOMO orbital is located at the naphthalene group. The obtained data are in agreement with the experimentally measured spectrum presented in Figure 1.

It should be noted that the theoretical spectra are shifted in relation to the experimental ones to the red wavelength side due to the regularity of the DFT methodology, although the shape of the calculated spectra is in agreement with the measured one (see Figure 1 and Figure S5). The spectral shift and apparent inconsistencies may be caused by ICT occurring between IN-O8-Cl and the solvent molecules, as well as by electron–phonon interaction present in the investigated system, which was not taken into account during quantum-chemical calculations. The HOMO and LUMO orbitals of the molecule in the excited state have exactly the same shape as that calculated for the molecule in ground state and presented in Figure S4. The $\Delta E_{\text{HOMO-LUMO}}$ value calculated for IN-O8-Cl in its excited state in the solvent environment decreases compared with the values in the ground state. The $\Delta E_{\text{HOMO-LUMO}}$ of the IN-O8-Cl molecule in the gas phase excited state also drastically decreases.

The theoretically found values of excited and ground state dipole moments in the gas phase as well as in four different solvents are presented in Table 2. The calculated ground state dipole moment is found to be higher than the experimentally obtained one. This is usually the case in molecules having long carbon chain. This could be attributed to the fact that in the modeled system the inhomogeneous electronic distribution through the molecule is overestimated compared with that of the real structure. Also, the differences between theoretical and experimental values of dipole moment arise due to the incompleteness of the used basis set and inappropriate nature of the chosen DFT functional. An appreciable change in dipole moment has been observed when we move from gas phase to solvent phase. In polar solvent, the solute is significantly polarized compared with that of nonpolar solvent. One may observe an increase in dipole moment moving from nonpolar to polar solvents, and it complies with the experimental data.

Analyzing the data obtained theoretically for the excited state dipole moment of the IN-O8-Cl, one may see that the first excited state dipole moment is lower than the ground state dipole moment. This means that in excitation process of the IN-O8-Cl molecule charge transfer appears to occur between molecules. The CPCM methodology used in presented work does not take into account the mentioned processes. It may be investigated by applying a discrete local field model implemented in our previous work.³⁹ The conformational changes of the molecular structure during photoexcitation are affected by the occurrence of the ICT which is not taken into account using the CPCM model to investigate the solvent effects. Even in the gas phase, the excited state dipole moment is lower than the one in ground state. This confirms that the IN-O8-Cl interacts with the other molecules exchanging charges, which is not modeled in presented work.

3.4. Steady-State Results in Aqueous Micellar Environment. The absorption spectra of IN-O8-Cl in aqueous solution with varying concentrations of SDS, CTAB, and TX-100 are shown in Figure 3. The IN-O8-Cl exhibits broad low energy absorption bands at 318 and 329 nm in bulk water. It is observed that on addition of surfactants (studied in this paper) there is an increase in absorbance along with a minor bathochromic shift in the first absorption band $\sim 2\text{--}3$ nm in the aqueous micellar environment indicating that the polarity in

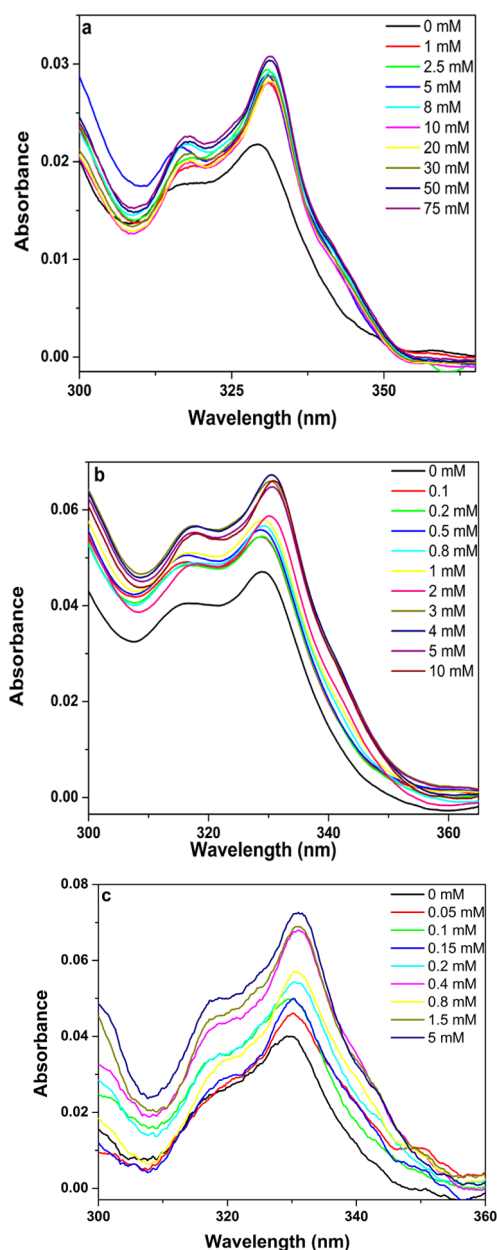


Figure 3. Steady state UV–vis absorption spectra of IN-O8-Cl in aqueous solution with varying concentrations of (a) SDS, (b) CTAB, and (c) TX-100.

the vicinity of the probe is slightly lower than that of the pure aqueous form.^{40–43} Addition of SDS causes a minor enhancement in both bands with a small red shift in the 329 nm band. A similar change was observed for triarylmethane (TPM) dyes bound to polyelectrolytes.⁴⁴ Similarly, a minor enhancement was observed in CTAB and TX-100.

In aqueous solution, IN-O8-Cl shows a strong fluorescence with emission maximum at 359 nm. With the addition of surfactants, significant spectral changes are observed in all the three environments as shown in Figure 4. The emission band gets blue-shifted to 353 nm in SDS and 354 nm in TX-100 micelles. The enhancement is larger in the neutral TX-100 micelles compared with anionic SDS micelles. The increase in fluorescence intensity along with the blue shift in the presence of anionic and neutral micelles compared with that of bulk water could be attributed to certain factors such as dipole

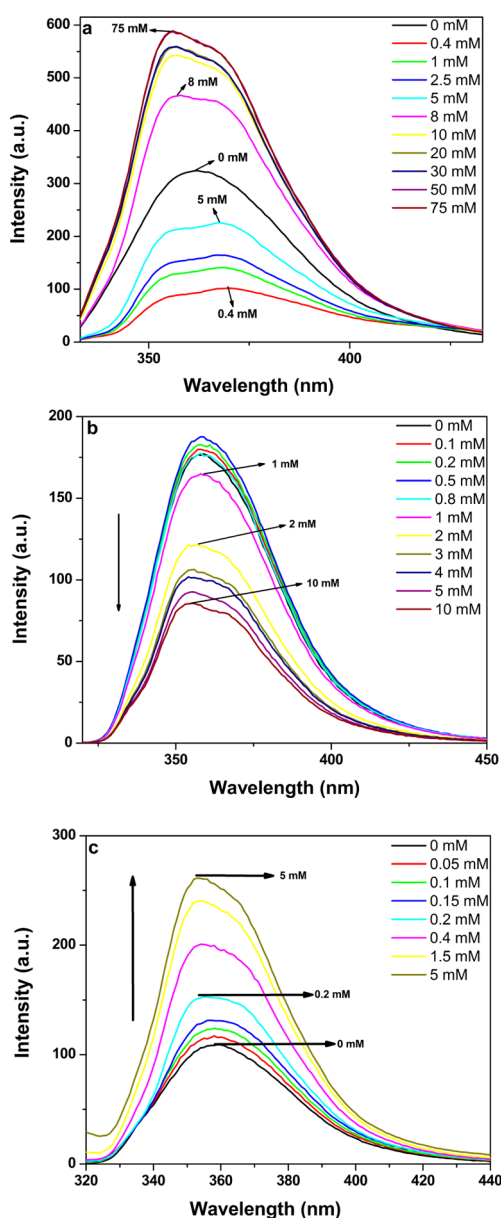


Figure 4. Emission spectra of IN-O8-Cl in aqueous solution with varying concentration of (a) SDS, (b) CTAB, and (c) TX-100.

moment and hydrogen bonding with water. The excited state is more polar than the ground state. So the excited state is less stable than the ground state in the less polar environment of the micelles than in water. This causes an increase in energy gap between the excited state and ground state, which would hinder the rate of nonradiative deactivation, resulting an increase in intensity with a consequent blue shift in emission in SDS and TX-100 micelles.

The other attributing factor is the formation of hydrogen bonds with water, which could quench the emission (as observed in SDS at pre-micellar concentrations, Figure 4a) due to an increase in nonradiative decay. But as the probe IN-O8-Cl moves from bulk water to micelles, the hydrogen bonding reduces due to the less polar environment of the micelles, thereby reducing the nonradiative transitions leading to the enhancement in SDS micelles. As we have observed the initial quenching followed by enhancement in intensity in SDS micelles, we have calculated and determined the change in

fluorescence quantum yield with increasing concentration of SDS, and variations in quantum yield along with nonradiative decay are shown in Figure S6.

In CTAB, no perceptible change in intensity of the fluorescent spectrum of IN-O8-Cl below CMC was observed. However, beyond CMC, there is gradual decrease in fluorescence intensity (Figure 4b) accompanied by a shift in fluorescence emission maximum. The decrease in the fluorescence intensity in the presence of CTAB micelles could be attributed to Br^- induced fluorescence quenching.⁴⁵ Hypsochromic shift of the fluorescence band along with an enhancement or reduction (SDS or TX-100 vs CTAB) of fluorescence intensity reflects that the microenvironment around the probe in surfactant solution is quite different from that in bulk aqueous phase. The hypsochromic shift indicates that the polarity in micellar solutions is lower compared with pure aqueous solution, and the variations in intensity suggest incorporation of IN-O8-Cl to SDS, CTAB, and TX-100. This change viewed in spectral properties can be attributed to overall change in viscosity or polarity.⁴⁶

3.5. Edge Excitation Red Shift (EERS). In the present study, the difference in the wavenumber (cm^{-1}) between the emission maximum obtained with excitation at 300 and 350 nm of the IN-O8-Cl in bulk and micellar solution is used to express EERS. As seen from Table 3, the emission spectrum of IN-O8-

Table 3. Spectroscopic Data of IN-O8-Cl in Bulk Water and Different Surfactant Systems

medium	emission maximum (nm)		EERS (cm^{-1})
	$\lambda_{\text{ex}} = 300 \text{ nm}$	$\lambda_{\text{ex}} = 350 \text{ nm}$	
bulk	359	366	533
75 mM SDS	353	365	916
10 mM CTAB	356	367	842
5 mM TX-100	354	365	931

Cl shows considerable dependence on excitation wavelength. The EERS values obtained for IN-O8-Cl in bulk water and at concentration higher than CMC for SDS, CTAB, and TX-100 surfactant systems are given in Table 3. The magnitude of EERS of IN-O8-Cl in bulk water solution is 533 cm^{-1} and in micellar environments is 916, 842, and 931 cm^{-1} for SDS, CTAB, and TX-100, respectively. The increase in magnitude of EERS is due to decrease in the solvent reorganization rate in response to the change in a concentration of ionic and neutral surfactant in the solution, whereas the increase in magnitude of EERS could be attributed to the fact that the viscosity around the probe in micellar systems increases. The interfacial region being the most viscous region is a suitable site for solubilization. This suggests that IN-O8-Cl is restricted in an inhomogeneous micellar environment, presumably at the water–micelle interface or deeper, in all the three environments.

3.6. Microenvironment around and Probable Location of the Probe Molecule. To further understand the interactions between probe molecule and different micelles, we have calculated the binding constant (K_b) from the fluorescence intensity plots. The method used for calculating the binding constant in SDS and TX-100 has been discussed in our earlier works.⁴⁷ The binding for CTAB with IN-O8-Cl has been calculated using the equation.^{48,49}

$$\log(F_0 - F)/F = \log K_b + n \log[Q] \quad (1)$$

where n is the number of binding sites and K_b is the binding constant, which can be determined from the slope and the intercepts of $\log(F_0 - F)/F$ vs $\log[Q]$.

Table 4 gives the value of K_b in all the three micellar environments using these two methods. The high K_b values in

Table 4. Different Solvent Parameters, Spectral Data, Binding Constant, Change in Gibbs' Free Energy of IN-O8-Cl in Different Micellar Environments

solvent	ϵ	η	$E_T(30)$	$\bar{\nu}_a - \bar{\nu}_f$ (cm^{-1})	K_b (L mol^{-1})	ΔG (kJ mol^{-1})
bulk water	80.00	1.33	63.10	2521		
SDS	10.9	1.41	37.67	1828	2.06×10^5	-30.52
CTAB	44.91	1.33	51.40	2121	0.41×10^3	-14.94
TX-100	17.6	1.39	40.29	1883	9.43×10^5	-34.31

SDS and TX-100 could be considerable due to increase in the fluorescence intensity of IN-O8-Cl along with a hypsochromic shift upon addition of SDS and TX-100 and above CMC (Figure 4a,c). In CTAB, we calculated the number of binding sites ($n = 1.09$) between IN-O8-Cl and CTAB, which is approximately equal to 1, indicating that there is only one binding site. Arikan et al.^{50,51} and many others obtained a similar order of binding constant for CTAB micelles. The higher binding constant in nonionic micelles (TX-100) and anionic micelles (SDS) could be due to stronger hydrogen or electrostatic bonding at the micellar head in the palisade layer compared with the hydrophobic binding in CTAB as it can be seen in Figure 5. Furthermore, the higher value of the binding constant for the probe in the nonionic TX-100 micelles is reflective of the fact that in contrast to the ionic micelles, hydrophobic interactions contribute to stronger binding of the dye to the neutral micelles due to TX-100 having a chain like structure with an iso-octyl phenyl group at one end. The Gibbs' free energy changes for the probe–micelle binding process in different micelles were calculated by the following equation at room temperature:

$$\Delta G = -RT \ln(K_b) \quad (2)$$

where $R = 8.314 \text{ J K}^{-1} \text{ mol}^{-1}$ is the universal constant, T is the room temperature in kelvin, and ΔG is the Gibbs' free energy

in kJ mol^{-1} . The Gibbs' free energies for SDS, CTAB, and TX-100 are tabulated in Table 4. The negative value indicates spontaneous binding in general but more favorable binding for inclusion in TX-100 micelles comparatively among all micelles.

Microenvironment such as polarity ($E_T(30)$), dielectric constant (ϵ), and refractive index (η) of biomimicking environments could be determined using fluorescent probes.^{52,53} By studying the spectral properties of IN-O8-Cl in pure solvents of known polarities and comparing them with spectral properties in micellar environments such parameters could be estimated.^{1,54,55} The micropolarity is a solvent parameter conveyed in equivalent scale of $E_T(30)$ correlating the fluorescence behavior of the probe in micellar systems to that in homogeneous solvents of varying polarities.^{53,56,57} The procedure used to determine the microenvironment for various micellar systems is given in our previous work.^{47,58}

The plots of Stoke's shifts of IN-O8-Cl in different homogeneous solvents against $E_T(30)$, refractive index, and dielectric constant are shown in Figure 6. Using this plot and the Stoke's shift values of IN-O8-Cl presented in Table S1, microenvironment around the probe has been estimated by interpolating the values of Stoke's shift of IN-O8-Cl in different micellar systems on the calibration curve, and the values are tabulated in Table 4. We have also observed an increase in refractive index and decrease in dielectric constant compared with bulk water suggesting that the molecule is in restricted environment.

It is observed that the micropolarity is very similar for IN-O8-Cl in the SDS and TX-100 micellar environments studied at concentrations higher than CMC. The reported $E_T(30)$ values of water, ethanol, and *n*-heptane are 63.1, 51.9, and 31.3 kcal mol^{-1} , respectively. Our estimated $E_T(30)$ values for TX-100 and SDS are lower than that of ethanol and higher than that of *n*-heptane; our values being much higher than *n*-heptane rules out the possibility of the probe penetrating into the core of the micelles. Finally, we could conclude that SDS/TX-100 penetrates deeper into micelle, maybe between the headgroup and first few carbons. In CTAB, it is at the water–micelle interface.

3.7. Effect of Ionic and Neutral Micelles on IN-O8-Cl Fluorescence Lifetime. Besides steady state studies, it is important to get an idea about excited state photophysical

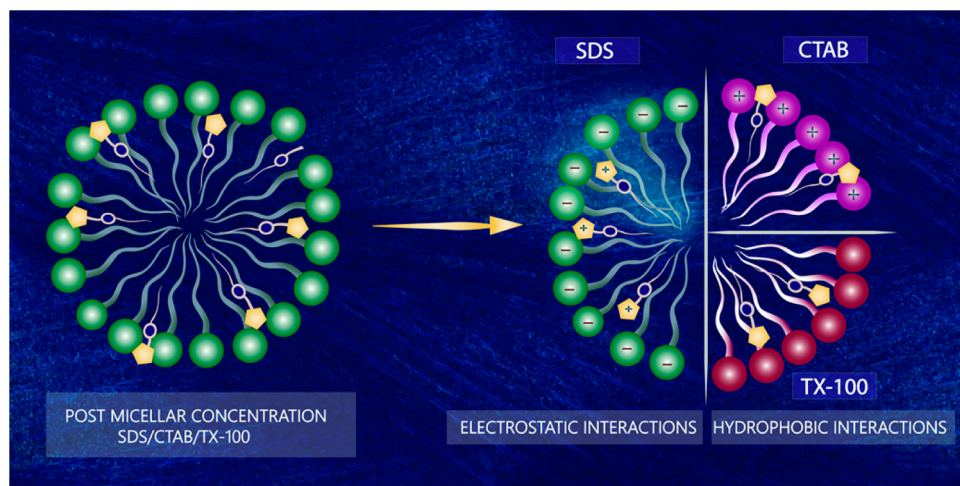


Figure 5. Illustration of electrostatic and hydrophobic interaction of IN-O8-Cl in different micellar environments at concentrations higher than CMC.

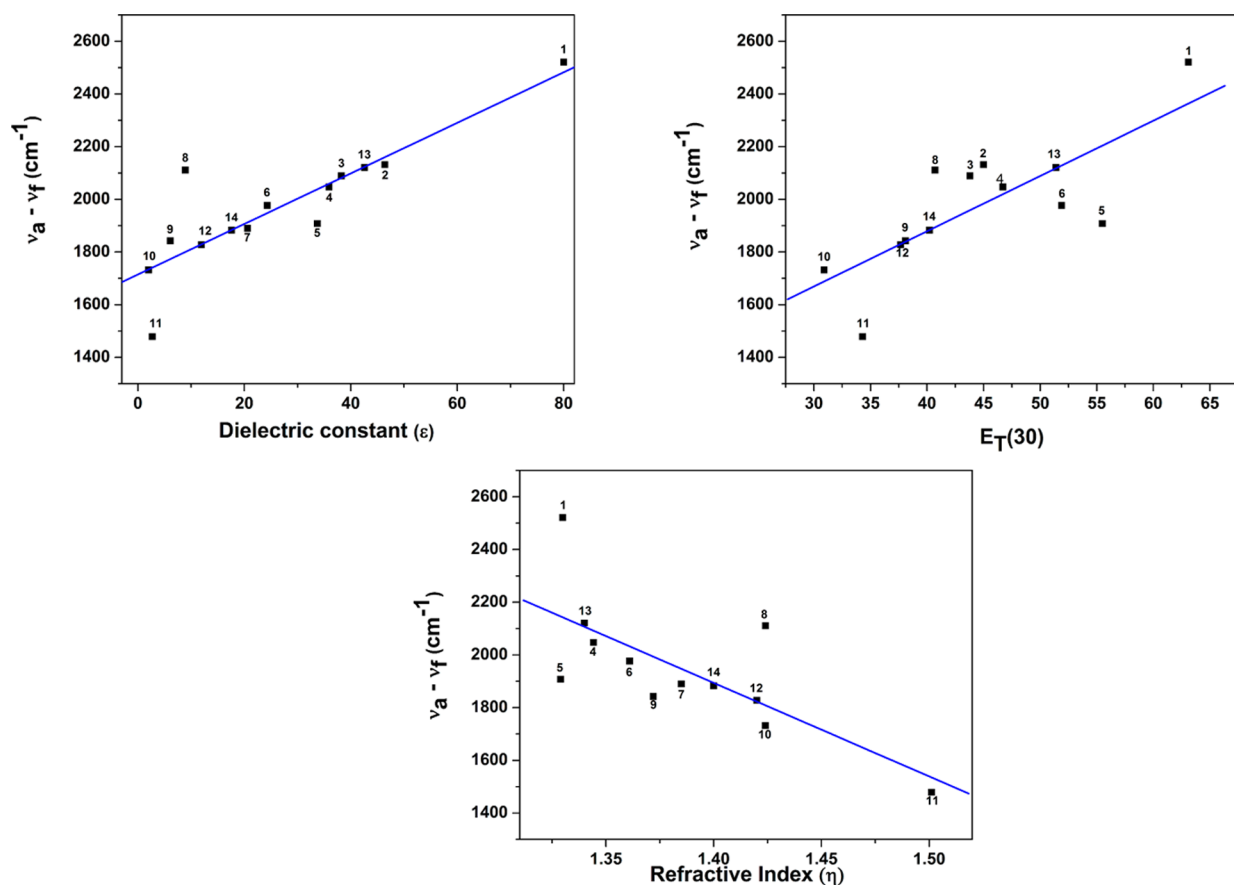


Figure 6. Stoke's shift vs solvent dielectric constant, $E_T(30)$, and refractive index for IN-O8-Cl in (1) Water, (2) DMSO, (3) DMF, (4) Acetonitrile, (5) Methanol, (6) Ethanol, (7) Isopropanol, (8) DCM, (9) Ethyl Acetate, (10) Cyclohexane, (11) Benzene, (12) SDS, (13) CTAB, and (14) TX-100.

processes that can be understood using time-resolved fluorescence measurements. Fluorescence lifetime measurements not only serve as an excellent indicator to explore the environment around the probe^{54,59,60} but also locate the probe in the micellar environment. Further, in order to determine the interactions between the probe and micelle, the excited state lifetimes of a fluorophore in micellar solutions have been studied.^{54,61–63} In aqueous solution of IN-O8-Cl, the emission decay ($\lambda_{ex} = 300$ nm) monitored at different emission wavelengths shows a biexponential behavior. Such biexponential behavior in micellar systems is due to the presence of hydrogen bonds forming with surrounding solvent.⁵⁴

Multiexponential decay was observed with a longer lifetime component depending upon the type of the surfactant on addition of successive surfactants. Figure 7 depicts the fluorescence decay profile of IN-O8-Cl in water and different micellar environments at highest concentrations above CMC. It is evident from Figure 7 that the fluorescent lifetime decay in cationic CTAB is slower than that in anionic SDS and nonionic TX-100. The lifetime in CTAB decreases to 4.73 ns compared with 9.91 ns in aqueous solution; this is due to the presence of heavy Br ion causing a decrease in the lifetime of IN-O8-Cl. The lifetime of IN-O8-Cl with addition of SDS or TX-100 is longer, due to the association of the fluorophore within SDS or TX-100 micelles, also indicating that the probe molecule resides inside the more viscous micelles. The decrease of lifetime of IN-O8-Cl with CTAB occurs due to exit of the probe molecule from inside the micelle to the surface at

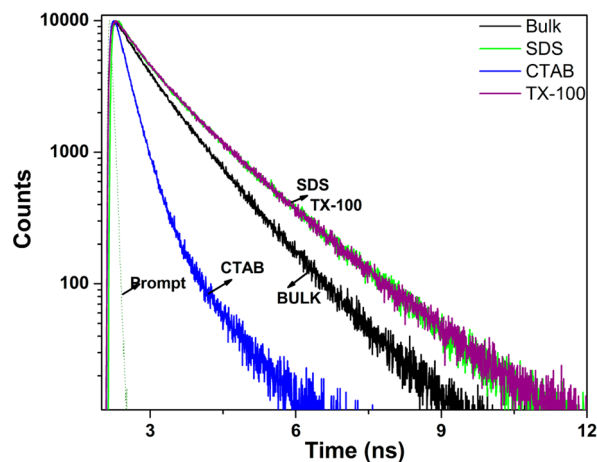


Figure 7. Time resolved fluorescent decay of IN-O8-Cl in bulk water and aqueous micellar environments ($\lambda_{ex} = 300$ nm and $\lambda_{em} = 375$ nm).

concentrations higher than CMC. The larger lifetime in anionic micelles may be because the molecule resides deep inside SDS micelles, which was also inferred from the steady state and microenvironment measurements.

Decay of IN-O8-Cl fluorescence in micellar systems exhibits multiexponential fitting. Multiexponential fluorescence decay for a probe is usually due to the presence of the probe in different polarity regions. Drawing meaningful conclusions in micellar systems often becomes tough when the fluorescence

decays are found to be multiexponential in nature. We choose to use the average fluorescence lifetime given by eq 2 of SI because it is an important parameter for understanding the dynamic motion of the probe in micellar systems, instead of placing too much stress on the individual magnitudes of the decay constants. The average lifetime values of IN-O8-Cl in all the micellar environments, thus estimated, are tabulated in Table S2. Fluorescence lifetime decays of IN-O8-Cl in aqueous solution with varying concentrations of different surfactants (SDS, CTAB, and TX-100) are shown in Figure S7.

Experimentally calculated values of lifetimes, taken at almost 10 times the CMC of SDS and TX-100, are significantly longer than those observed in water, indicating that the probe is not soluble in bulk water surrounding the micelles, but the longer and shorter lifetime component could be attributed to the presence of the probe in stern layer and water–micellar interface in SDS or TX-100 micellar environments. The longer lifetime component assumes values close to 14 ns, indicating the suppression of nonradiative pathways of de-excitation when IN-O8-Cl interacts with both anionic and neutral micelles. However, for SDS, the occurrence of the third (lowest) lifetime component could indicate that the probe could be partially exposed to the aqueous environment, whereas for CTAB from the pre-exponential factors it could be concluded that the majority of the probe molecules (80–95%) are solubilized at the water–micellar interface and only 5–20% are at the stern layer.

The quantum yield QY (ϕ) is calculated from the total fluorescence emission area over the whole spectral range, using quinine sulfate dication in bulk water as standard. The radiative (κ_r) and nonradiative (κ_{nr}) rate constants were calculated from the fluorescence quantum yield (ϕ) and average lifetimes (τ) using the relations

$$\kappa_r = \phi / \langle \tau \rangle \quad (3)$$

$$\kappa_{nr} = (1 - \phi) / \langle \tau \rangle \quad (4)$$

The parameters are tabulated in Table 5.

Table 5. Quantum Yields and Radiative and Nonradiative Rate Constants of IN-O8-Cl in Aqueous and Micellar Environments

surfactant	concentration (mM)	ϕ	κ_r (10^8 s^{-1})	κ_{nr} (10^8 s^{-1})
SDS	0	0.12	0.12	0.91
	0.4	0.06	0.09	1.50
	8.0	0.13	0.11	0.70
	75.0	0.15	0.12	0.68
CTAB	0.1	0.11	0.11	0.91
	1.0	0.09	0.09	0.98
	5.0	0.04	0.07	1.60
TX-100	0.05	0.12	0.12	0.88
	0.2	0.10	0.10	0.83
	5.0	0.12	0.10	0.69

Initially at pre-micellar concentrations of SDS, formation of nonfluorescent ion pairs causes a decrease in fluorescent intensity, which is reflected in the decrease in QY compared with that of bulk. The QY remains constant (~ 0.06) at pre-micellar concentration of SDS, but at CMC, there is remarkable increase in QY (~ 0.13), and it remains almost constant as concentration of SDS increases. In TX-100 as the concentration increases, the QY pretty much remains constant.

The QY values of SDS and TX-100 are in agreement with the decrease in nonradiative relaxation and increase in the fluorescence intensity at concentrations higher than CMC, whereas in CTAB the QY remains constant in bulk and at pre-micellar concentrations, but at and above CMC, a continuous decrease in QY was observed, which is in concert with the decrease in fluorescence intensity and increase in the nonradiative relaxation

3.8. Time-Resolved Anisotropy Study. In order to understand the effect of micellar environment on rotational correlation time of the fluorophore in organized assemblies,^{1,40} we have recorded fluorescence anisotropy time dependent decay. In bulk water, the anisotropy decay is monoexponential, and the time constant is 0.45 ns. In order to contrast the constraint imposed on the probe in the micellar system relative to bulk solution, rotational correlation times were calculated. In SDS and CTAB, IN-O8-Cl shows single exponential anisotropy decay. The observed single exponential anisotropy decay rules out the probability of the probe rotating within or along with the micelle in SDS and CTAB micellar media. In SDS and CTAB micelles, monoexponential decays of IN-O8-Cl might imply solubilization of the probe in a single region, either in the head region or in the core region of the micelles. The decay in TX-100 micelles follows a biexponential pattern. The biexponential anisotropy decay $r(t)$ in micelles can be represented as follows

$$r(t) = r_0 [a_1 \exp(-t/\tau_{1r}) + a_2 \exp(-t/\tau_{2r})] \quad (5)$$

where r_0 is the limiting anisotropy, τ_{1r} and τ_{2r} are the two reorientation times of the probe in TX-100 micelles, and a_1 and a_2 are the corresponding relative amplitudes.

The restriction imposed on the fluorophore in the micellar systems relative to bulk aqueous solution can be compared by calculating the average rotational correlational times using the eq 2 (SI). The anisotropy decay parameters in bulk and micellar systems are summarized in Table S3, whereas Figure 8 shows the anisotropy decay of IN-O8-Cl in SDS, CTAB and TX-100 micellar solutions.

An increase in the sternness of the nearby environment of a probe results in a slower rotational correlation time. The average rotational times of IN-O8-Cl in all micellar environments, SDS (790 ps), CTAB (1280 ps), and TX-100 (2740 ps),

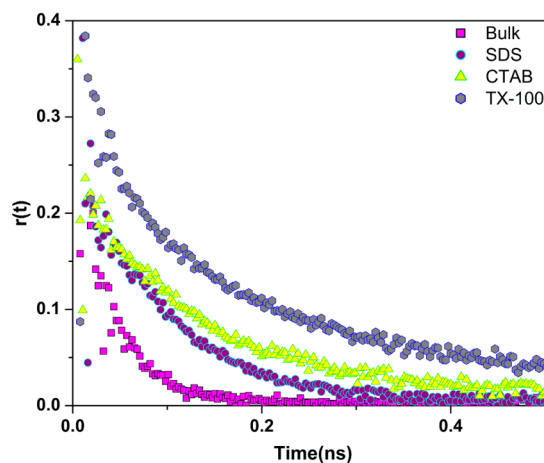


Figure 8. Time resolved fluorescence anisotropy decay profiles for IN-O8-Cl in bulk, 75 mM SDS, 50 mM CTAB, and 5 mM TX-100 micellar solution, $\lambda_{ex} = 300 \text{ nm}$, $\lambda_{em} = 360 \text{ nm}$.

are slower compared with pure aqueous solution, suggesting that the probe is restricted motionally in the micellar environment compared with bulk water.

In micelles, biexponential decays of IN-O8-Cl might imply two different distributions of the fluorophore. Biexponential anisotropy decay in the case of TX-100 implies that the coefficients a_1 and a_2 amount to the possibility of finding the probe in the headgroup region and the core region. The possibility of finding the probe is low in the core region because it does not satisfy the condition $a_2 \gg a_1$, in agreement with our investigation described in section 3.5. Hence, the biexponential decay in TX-100 is not because of the probability of the probe being solubilized either at the head or in the core but because it experiences different kinds of motion.^{64–67} The probe molecule, depending on its position, undergoes fast wobbling motion in an imaginary cone described by semiangle θ and also slow lateral diffusion at or near the interface of the micelle. These two motions are coupled to the rotation of the micelle. The fast and slow reorientation times are related to the time constants for wobbling motion, τ_W , lateral diffusion, τ_L , and whole rotation of the micelle, τ_M , by the following relations, assuming that the fast and slow motions are separable,

$$1/\tau_{\text{slow}} = 1/\tau_L + 1/\tau_M \quad (6)$$

$$1/\tau_{\text{fast}} = 1/\tau_W + 1/\tau_{\text{slow}} \quad (7)$$

where τ_{slow} and τ_{fast} are the observed slow and fast components. The time constant for the overall rotation of the micelle has been obtained using Stokes–Einstein–Debye (SED) hydrodynamic theory with the stick boundary condition,⁶⁸

$$\tau_M = \eta V_h / (KT) \quad (8)$$

where η is the viscosity of the medium and V_h is the hydrodynamic volume of the micelle obtained from hydrodynamic radius (r_M) of the micelle (calculated from eq 9). K and T are the Boltzmann constant and absolute temperature, respectively,

$$r_M = (3N_{\text{agg}}(27.4 + 26.9n)/(4\pi))^{1/3} \quad (9)$$

and n is the number of carbons of the surfactant's alkyl chain. The hydrodynamic radius of TX-100 micelle in water is calculated to be 2.73 nm. The calculated τ_M value is of much higher magnitude compared with that of τ_1 and τ_2 values, thereby proving that the decay is not due to the overall rotation but attributed the fluorescence depolarization becoming negligible due to the long reorientation time for the overall rotation of the micelles. In order to get a fair interpretation about the possible location of the probe the order parameter (S) has been calculated. The value of S is obtained from the relative amplitude of the slow component by using the equation

$$S^2 = a_1 \quad (10)$$

The magnitude of the S is a measure of spatial restriction. The value of S obtained is 0.68; this high value of order parameter indicates restricted motion. Compared with that of bulk water, the anisotropy decay of IN-O8-Cl bound to SDS, CTAB, and TX-100 micelles is found to be slower. The motional restriction of IN-O8-Cl molecules follows the order TX-100 > CTAB > SDS. It can be thus concluded that IN-O8-Cl is bound to the ionic and nonionic micelles. The fluorophore is restricted more motionally in TX-100 environment of micelles, which could be due to TX-100 having a chain like structure with an iso-octyl

phenyl group at one end; this chain structure facilitates better binding of the probe with TX-100 micelles.

4. CONCLUSIONS

In this paper the values of the ground and excited state dipole moment of IN-O8-Cl molecule were determined. The excited state dipole moment is much higher than that of ground state. From the DFT quantum chemical calculation, the effect is completely different, which implies that the conformational changes of the IN-O8-Cl during photoexcitation are affected by the ICT process, which is not taken into account using CPCM model. This confirms that IN-O8-Cl, even in the gas phase, interacts with neighboring molecules exchanging charges, which is not modeled in presented work. The weak change in absorption spectra in comparison to that of the emission spectra indicates that the molecule is less polarized by the polar solvents in the ground state than in the excited state. These results firmly suggest that the nonbonding electrons are not involved in $n \rightarrow \pi^*$ transition but involved in $\pi \rightarrow \pi^*$ transition due to charge transfer. From steady state spectral data of IN-O8-Cl, the EERS, binding constant, micropolarity values, and also probable location of the probe were calculated. Time-resolved studies revealed that the fluorescence lifetime decay shows multiexponential behavior in bulk and micellar solution, whereas anisotropy decay of IN-O8-Cl in bulk, SDS, and CTAB are monoexponential, but the decay in TX-100 is biexponential. Finally, from the steady state and time-resolved fluorescence techniques, various spectral parameters such as micropolarity, refractive index, dielectric constant, EERS, binding constant, fluorescence lifetime, and anisotropy have been determined. One may be able to conclude that IN-O8-Cl binds strongly to the micelles and resides at the water–micellar interface for CTAB, whereas it resides between the head and first few carbons for SDS and TX-100.

■ ASSOCIATED CONTENT

Supporting Information

The Supporting Information is available free of charge on the ACS Publications website at DOI: 10.1021/acs.jpca.6b05864.

Dipole moment analysis, the ground state HOMO and LUMO orbitals and computed MEP surface in gas, and fluorescence lifetime of IN-O8-Cl. Original copies of ¹H NMR and ¹³C NMR spectra of Compound 4, 5, 7 are also included. (PDF)

■ AUTHOR INFORMATION

Corresponding Authors

*Tel: +420 773207978. E-mail: ytejvarma@gmail.com.

*Tel: +48 343614919, int. 271. E-mail: m.makowska@ajd.czesz.pl.

*Tel: +91 1596515288. E-mail: ddpant@pilani.bits-pilani.ac.in.

Notes

The authors declare no competing financial interest.

■ ACKNOWLEDGMENTS

We acknowledge University grants commission (UGC) and DST, New Delhi, for major research project to D.D.P., and T.V.Y. thanks Birla Institute of Technology and Sciences, Pilani Campus, for Research fellowship. D.A. is thankful to DST, New Delhi, for JRF, R.S. is thankful to DST, New Delhi, for major research project. Quantum chemical calculations have been

carried out in Wroclaw Centre for Networking and Supercomputing (<http://www.wcss.wroc.pl>) (Grant no. 171).

REFERENCES

- (1) Lakowicz, J. R. *Principles of Fluorescence Spectroscopy*; Kluwer Academic: New York, 1999.
- (2) Dobretsov, G. E. *Fluorescent Probes for Studying Cells, Membranes and Protein*; Nauka, Moscow, 1989 (in Russian).
- (3) Iniewski, K. *Smart Sensors for Industrial applications*; CRC Press: Boca Raton, FL, 2013.
- (4) Resch-Genger, U.; Grabolle, M.; Cavaliere-Jaricot, S.; Nitschke, R.; Nann, T. Quantum Dots versus Organic Dyes as Fluorescent Labels. *Nat. Methods* **2008**, *5*, 763–775.
- (5) Mihindukulasuriya, S. H.; Morcone, T. K.; McGown, L. B. Characterization of Acridone Dyes for Use in Four-Decay Detection in DNA Sequencing. *Electrophoresis* **2003**, *24*, 20–25.
- (6) Sun, Y.; Wei, S.; Zhao, Y.; Hu, X.; Fan, J. Interactions between 4-(2-dimethylaminoethoxy)-*N*-octadecyl-1,8-naphthalimide and Serum Albumins: Investigation by Spectroscopic Approach. *J. Lumin.* **2012**, *132*, 879–886.
- (7) Kar, C.; Ojha, B.; Das, G. A. Novel Amphiphilic Thiosemicarbazone Derivative for Binding and Selective Sensing of Human Serum Albumin. *J. Lumin.* **2013**, *28*, 339–344.
- (8) Rogers, R. D.; Seddon, K. R. Ionic Liquids - Solvents of the Future? *Science* **2003**, *302*, 792–793.
- (9) Anderson, J. L.; Armstrong, D. W.; Wei, G. T. Ionic Liquids in Analytical Chemistry. *Anal. Chem.* **2006**, *78*, 2892–2902.
- (10) Crank, J. A.; Armstrong, D. W. Towards a Second Generation of Ionic Liquid Matrices (ILMs) for MALDI-MS of Peptides, Proteins, and Carbohydrates. *J. Am. Soc. Mass Spectrom.* **2009**, *20*, 1790–1800.
- (11) Plechkova, N. V.; Seddon, K. R. Applications of Ionic Liquids in the Chemical Industry. *Chem. Soc. Rev.* **2008**, *37*, 123–150.
- (12) Welton, T. Room-Temperature Ionic Liquids. Solvents for Synthesis and Catalysis. *Chem. Rev.* **1999**, *99*, 2071–2083.
- (13) Giernoth, R. Task-Specific Ionic Liquids. *Angew. Chem., Int. Ed.* **2010**, *49*, 2834–2839.
- (14) Davis, J. H., Jr. Task-Specific Ionic Liquids. *Chem. Lett.* **2004**, *33*, 1072–1077.
- (15) Lee, S. Functionalized Imidazolium Salts for Task-Specific Ionic Liquids and Their Applications. *Chem. Commun.* **2006**, 1049–1063.
- (16) Katayanagi, H.; Hayashi, S.; Hamaguchi, H.; Nishikawa, K. Structure of an Ionic Liquid, 1-*n*-butyl-3-methylimidazolium iodide, Studied by Wide-angle X-ray Scattering and Raman Spectroscopy. *Chem. Phys. Lett.* **2004**, *392*, 460–464.
- (17) Mele, A.; Tran, C. D.; De Paoli Lacerda, S. H. The Structure of a Room-Temperature Ionic Liquid with and without Trace Amounts of Water: The Role of C_H...O and C_H...F Interactions in 1-*n*-butyl-3-methylimidazolium tetrafluoroborate. *Angew. Chem., Int. Ed.* **2003**, *42*, 4364–4366.
- (18) Shu, Y.; Liu, M.; Chen, S.; Chen, X.; Wang, J. New Insight into Molecular Interactions of Imidazolium Ionic Liquids with Bovine Serum Albumin. *J. Phys. Chem. B* **2011**, *115*, 12306–12314.
- (19) Chen, X. W.; Liu, J. W.; Wang, J. H. A Highly Fluorescent Hydrophilic Ionic Liquid as a Potential Probe for the Sensing of Biomacromolecules. *J. Phys. Chem. B* **2011**, *115*, 1524–1530.
- (20) Liu, H.; Zhang, L.; Chen, J.; Zhai, Y.; Zeng, Y.; Li, L. A Novel Functional Imidazole Fluorescent Ionic Liquid: Simple and Efficient Fluorescent Probes for Superoxide Anion Radical. *Anal. Bioanal. Chem.* **2013**, *405*, 9563–9570.
- (21) Galpothdeniya, W. I. S.; Das, S.; De Rooy, S. L.; Regmi, B. P.; Hamdan, S.; Warner, I. M. Fluorescein-based Ionic Liquid Sensor for Label-Free Detection of Serum Albumins. *RSC Adv.* **2014**, *4*, 17533–17540.
- (22) Galpothdeniya, W. I. S.; McCarter, K. S.; De Rooy, S. L.; Regmi, B. P.; Das, S.; Hasan, F.; Tagge, A.; Warner, I. M. Ionic Liquid-based Optoelectronic Sensor Arrays for Chemical Detection. *RSC Adv.* **2014**, *4*, 7225–7234.
- (23) Yung, K. Y.; Schadock-Hewitt, A. J.; Hunter, N. P.; Bright, F. V.; Baker, G. A. 'Liquid Litmus': Chemosensory pH-Responsive Photonic Ionic Liquids. *Chem. Commun.* **2011**, *47*, 4775–4777.
- (24) Zhao, F.; Ma, M. L.; Xu, B. Molecular Hydrogels of Therapeutic Agents. *Chem. Soc. Rev.* **2009**, *38*, 883–891.
- (25) Becke, A. D. Density-functional Thermochemistry. III. The Role of Exact Exchange. *J. Chem. Phys.* **1993**, *98*, 5648–5652.
- (26) Lee, C.; Yang, W.; Parr, R. G. Development of the Colle-Salvetti Correlation-Energy Formula into a Functional of the Electron Density. *Phys. Rev. B: Condens. Matter Mater. Phys.* **1988**, *37*, 785–789.
- (27) Frisch, M. J.; Trucks, G. W.; Schlegel, H. B.; Scuseria, G. E.; Robb, M. A.; Cheeseman, J. R.; Scalmani, G.; Barone, V.; Mennucci, B.; Petersson, G. A.; Nakatsuji, H.; Caricato, M.; Li, X.; Hratchian, H. P.; Izmaylov, A. F.; Bloino, J.; Zheng, G.; Sonnenberg, J. L.; Hada, M.; Ehara, M.; Toyota, K.; Fukuda, R.; Hasegawa, J.; Ishida, M.; Nakajima, T.; Honda, Y.; Kitao, O.; Nakai, H.; Vreven, T.; Montgomery, J. A., Jr.; Peralta, J. E.; Ogliaro, F.; Bearpark, M.; Heyd, J. J.; Brothers, E.; Kudin, K. N.; Staroverov, V. N.; Kobayashi, R.; Normand, J.; Raghavachari, K.; Rendell, A.; Burant, J. C.; Iyengar, S. S.; Tomasi, J.; Cossi, M.; Rega, N.; Millam, J. M.; Klene, M.; Knox, J. E.; Cross, J. B.; Bakken, V.; Adamo, C.; Jaramillo, J.; Gomperts, R.; Stratmann, R. E.; Yazyev, O.; Austin, A. J.; Cammi, R.; Pomelli, C.; Ochterski, J. W.; Martin, R. L.; Morokuma, K.; Zakrzewski, V. G.; Voth, G. A.; Salvador, P.; Dannenberg, J. J.; Dapprich, S.; Daniels, A. D.; Farkas, O.; Foresman, J. B.; Ortiz, J. V.; Cioslowski, J.; Fox, D. J. *Gaussian 09*, revision D.01; Gaussian, Inc.: Wallingford, CT, 2009.
- (28) Schlegel, H. B. Optimization of Equilibrium Geometries and Transition Structures. *J. Comput. Chem.* **1982**, *3*, 214–218.
- (29) Hohenberg, P.; Kohn, W. Inhomogeneous Electron Gas. *Phys. Rev. B* **1964**, *136*, 864–871.
- (30) Parr, R. G.; Yang, W. *Density-Functional Theory of Atoms and Molecules*; Oxford University Press: New York, 1989.
- (31) Barone, V.; Cossi, M. Quantum Calculation of Molecular Energies and Energy Gradients in Solution by a Conductor Solvent Model. *J. Phys. Chem. A* **1998**, *102*, 1995–2001.
- (32) Cossi, M.; Rega, N.; Scalmani, G.; Barone, V. Energies, Structures, and Electronic Properties of Molecules in Solution with the C-PCM Solvation Model. *J. Comput. Chem.* **2003**, *24*, 669–681.
- (33) Miertus, S.; Tomasi, J. Approximate Evaluations of the Electrostatic Free Energy and Internal Energy Changes in Solution Processes. *Chem. Phys.* **1982**, *65*, 239–245.
- (34) Miertus, S.; Scrocco, E.; Tomasi, J. Electrostatic Interaction of a Solute with a Continuum. A Direct Utilization of ab initio Molecular Potentials for the Prediction of Solvent Effects. *Chem. Phys.* **1981**, *55*, 117–129.
- (35) Tway, P. C.; Love, L. J. C. Photophysical Properties of Benzimidazole and Thiabendazole and Their Homologs. Effect of Substituents and Solvent on the Nature of the Transition. *J. Phys. Chem.* **1982**, *86*, 5223–5226.
- (36) Varma Y, T.; Joshi, S.; Pant, D. D. Solvatochromatic Shift of Absorption and Fluorescence Spectra of 6-methoxyquinoline: Estimation of Ground and Excited State Dipole Moments. *J. Mol. Liq.* **2013**, *179*, 7–11.
- (37) Joshi, S.; Bhattacharjee, R.; Varma Y, T.; Pant, D. D. Estimation of Ground and Excited State Dipole Moments of Quinidine and Quinidine Dication: Experimental and Numerical Methods. *J. Mol. Liq.* **2013**, *179*, 88–93.
- (38) Sharma, R.; Joshi, S.; Bhattacharjee, R.; Pant, D. D. Solvent Effect on Absorption and Fluorescence Spectra of Cinchonine and Cinchonidine Dications: Estimation of Ground and Excited State Dipole Moments by Experimental and Numerical Studies. *J. Mol. Liq.* **2015**, *206*, 159–164.
- (39) Reis, H.; Makowska-Janusik, M.; Papadopoulos, M. G. Nonlinear Optical Susceptibilities of Poled Guest-Host Systems: A Computational Approach. *J. Phys. Chem. B* **2004**, *108*, 8931–8940.
- (40) Das, P.; Mallick, A.; Haldar, B.; Chakrabarty, A.; Chattopadhyay, N. Effect of Nanocavity Confinement on the Rotational Relaxation Dynamics: 3-acetyl-4-oxo-6,7-dihydro-12*H* indolo-[2,3-*a*] quinolizine in Micelles. *J. Chem. Phys.* **2006**, *125*, 044516.

- (41) Das, P.; Sarkar, D.; Chattopadhyay, N. Photophysics of a β -carboline based non-Ionic Probe with Anionic and Zwitterionic Liposome Membranes. *Chem. Phys. Lipids* **2008**, *154*, 38–45.
- (42) Mahata, A.; Sarkar, D.; Bose, D.; Ghosh, D.; Das, P.; Chattopadhyay, N. Photophysics and Rotational Relaxation Dynamics of a β -carboline based Fluorophore in Cationic Alkyl Trimethyl Ammonium Bromide Micelles. *J. Colloid Interface Sci.* **2009**, *335*, 234–241.
- (43) Mahata, A.; Sarkar, D.; Bose, D.; Ghosh, D.; Girigoswami, A.; Das, P.; Chattopadhyay, N. Photophysics and Rotational Dynamics of a β -carboline Analogue in Nonionic Micelles: Effect of Variation of Length of the Head Group and the Tail of the Surfactant. *J. Phys. Chem. B* **2009**, *113*, 7517–7526.
- (44) Jones, G., II; Oh, G.; Goswami, K. The Photochemistry of Triarylmethane Dyes Bound to Polyelectrolytes: Photoinduced Electron Transfer Involving Bound Dye Monomers and Dimers. *J. Photochem. Photobiol., A* **1991**, *57*, 65–80.
- (45) Koner, A. L.; Mishra, P. P.; Jha, S.; Datta, A. The Effect of Ionic Strength and Surfactant on the Dynamic Quenching of 6-methoxyquinoline by Halides. *J. Photochem. Photobiol., A* **2005**, *170*, 21–26.
- (46) Hu, Z.; Margulis, C. J. Room-Temperature Ionic Liquids: Slow Dynamics, Viscosity, and the Red Edge Effect. *Acc. Chem. Res.* **2007**, *40*, 1097–1105.
- (47) Varma, Y. T.; Pant, D. D. Interaction of 6-methoxyquinoline with Anionic Sodium Dodecylsulfate Micelles: Photophysics and Rotational Relaxation Dynamics at different. *Spectrochim. Acta, Part A* **2016**, *158*, 9–17.
- (48) Tian, J. N.; Liu, J. Q.; Zhang, J. Y.; Hu, Z. D.; Chen, X. G. Fluorescence Studies on the Interactions of Barbaloin with Bovine Serum Albumin. *Chem. Pharm. Bull.* **2003**, *51*, 579–582.
- (49) Hu, Y. J.; Liu, Y.; Sun, T. Q.; Bai, A. M.; Lu, J. Q.; Pi, Z. B. Binding of Anti-Inflammatory Drug Cromolyn Sodium to Bovine Serum Albumin. *Int. J. Biol. Macromol.* **2006**, *39*, 280–285.
- (50) Arikan, B.; Tuncay, M. Micellar Effects and Reactant Incorporation in Reduction of Toluibine Blue by Ascorbic Acid. *Dyes Pigm.* **2005**, *64*, 1–8.
- (51) Gul, F.; Khan, A. M.; Shah, S. S.; Nazar, M. F. Spectroscopic Study of Alizarin Reds Binding with Cetyltrimethylammonium Bromide at Low Concentrations. *Color. Technol.* **2010**, *126*, 109–113.
- (52) Chakrabarty, A.; Mallick, A.; Haldar, B.; Das, P.; Chattopadhyay, N. Binding Interaction of a Biological Photosensitizer with Serum Albumins: A Biophysical Study. *Biomacromolecules* **2007**, *8*, 920–927.
- (53) Macgregor, R. B.; Weber, G. Estimation of the Polarity of the Protein Interior by Optical Spectroscopy. *Nature* **1986**, *319*, 70–73.
- (54) Mallick, A.; Haldar, B.; Chattopadhyay, N. Spectroscopic Investigation on the Interaction of ICT Probe 3-acetyl-4-oxo-6,7-dihydro-12H indolo-[2,3-a]quinolozine with Serum Albumins. *J. Phys. Chem. B* **2005**, *109*, 14683–14690.
- (55) Shannigrahi, M.; Bagchi, S. Dual Probe Solubilization in two Distinct Regions of Pure and Mixed Micelles: A Pico-Second Time Resolved Fluorescence Study. *Chem. Phys. Lett.* **2004**, *396*, 367–371.
- (56) Das, R.; Guha, D.; Mitra, S.; Kar, S.; Lahiri, S.; Mukherjee, S. Intramolecular Charge Transfer as Probing Reaction: Fluorescence Monitoring of Protein-Surfactant Interaction. *J. Phys. Chem. A* **1997**, *101*, 4042–4047.
- (57) Dennison, S. M.; Guharay, J.; Sengupta, P. K. Excited-State Intramolecular Proton Transfer (ESIPT) and Charge Transfer (CT) Fluorescence Probe for Model Membranes. *Spectrochim. Acta, Part A* **1999**, *55*, 1127–1132.
- (58) Tej Varma, Y.; Joshi, S.; Pant, D. D. Effect of Nanosize Micelles of Ionic and Neutral Surfactants on the Photophysics of Protonated 6-methoxyquinoline: Time-Resolved Fluorescence Study. *Spectrochim. Acta, Part A* **2015**, *138*, 818–826.
- (59) Paul, B. K.; Samanta, A.; Guchhait, N. Modulation of Excited State Intramolecular Proton Transfer Reaction of 1-hydroxy-2naphthadehyde in Different Supramolecular Assemblies. *Langmuir* **2010**, *26*, 3214–3224.
- (60) Sarker, N.; Das, N.; Das, S.; Datta, A.; Nath, D.; Bhattacharyya, K. Excited-State Intramolecular Proton Transfer of 2-(2'-hydroxyphenyl) benzimidazole in Micelles. *J. Phys. Chem.* **1995**, *99*, 17711–17714.
- (61) Maciejewski, A.; Kubicki, J.; Dobek, K. The Origin of Time-Resolved Emission Spectra (TRES) Changes of 4-Aminophthalimide (4-AP) in SDS Micelles. The Role of the Hydrogen Bond between 4-AP and Water Present in Micelles. *J. Phys. Chem. B* **2003**, *107*, 13986–13999.
- (62) Chattopadhyay, A.; Mukherjee, S.; Raghuraman, H. Reverse Micellar Organization and Dynamics: A Wavelength -Selective Fluorescence Approach. *J. Phys. Chem. B* **2002**, *106*, 13002–13009.
- (63) Prendergast, F. G. Time-Resolved Fluorescence Techniques: Methods and Applications in Biology. *Curr. Opin. Struct. Biol.* **1991**, *1*, 1054–1059.
- (64) Quitevis, E. L.; Marcus, A. H.; Fayer, M. D. Dynamics of Ionic Lipophilic Probes in Micelles: Picosecond Fluorescence Depolarization Measurements. *J. Phys. Chem.* **1993**, *97*, 5762–5769.
- (65) Wittouck, N.; Negri, R. M.; Ameloot, M.; De Schryver, F. C. AOT Reversed Micelles Investigated by Fluorescence Anisotropy of Cresyl Violet. *J. Am. Chem. Soc.* **1994**, *116*, 10601–10611.
- (66) Maiti, N. C.; Mazumdar, S.; Periasamy, N. Dynamics of Porphyrin Molecules in Micelles. Picosecond Time-Resolved Fluorescence Anisotropy Studies. *J. Phys. Chem.* **1995**, *99*, 10708–10715.
- (67) Krishna, M. M. G.; Das, R.; Periasamy, N.; Nityananda, R. Translational Diffusion of Fluorescent Probes on a Sphere: Monte Carlo Simulations, Theory, and Fluorescence Anisotropy Experiment. *J. Chem. Phys.* **2000**, *112*, 8502–8514.
- (68) Debye, P. *Polar Molecules*; Dover: New York, 1929.